






# UV to X-Ray Comptonization Delay in Mrk 493

Oluwashina Adegoke<sup>1</sup> , Gulab C. Dewangan<sup>2</sup> , Pramod Pawar<sup>2,3</sup> , and Main Pal<sup>4</sup>

<sup>1</sup>Department of Physics, Indian Institute of Science, Bangalore 560012, India; [oluwashinaa@iisc.ac.in](mailto:oluwashinaa@iisc.ac.in)

<sup>2</sup>Inter-University Center for Astronomy and Astrophysics, Pune 411007, India

<sup>3</sup>Swami Ramanand Teerth Marathwada University, Nanded 431606, India

<sup>4</sup>Centre for Theoretical Physics, Jamia Millia Islamia, New Delhi 110025, India

Received 2018 August 30; revised 2018 December 9; accepted 2018 December 17; published 2019 January 9

## Abstract

The broadband X-ray emission from type 1 active galactic nuclei, dominated by a power-law continuum, is thought to arise from repeated inverse Compton scattering of seed optical/UV photons by energetic electrons in a hot corona. The seed optical/UV photons are assumed to arise from an accretion disk, but direct observational evidence has remained elusive. Here we report the discovery of variations in the UV emission preceding the variations in the X-ray emission based on  $\sim 100$  ks *XMM-Newton* observations of the narrow-line Seyfert 1 galaxy Mrk 493. We find that the UV emission leads by  $\sim 5$  ks relative to the X-ray emission. The UV lead is consistent with the time taken by the UV photons to travel from the location of their origin in the accretion disk to the hot corona, and the time required for repeated inverse Compton scattering converting the UV photons into X-ray photons. Our findings provide the first direct observational evidence for the accretion disk being responsible for the seed photons for thermal Comptonization in the hot corona, and for constraining the size of the corona to  $\sim 20r_g$ .

**Key words:** galaxies: active – galaxies: individual (Mrk 493) – galaxies: Seyfert – X-rays: galaxies

## 1. Introduction

A substantial fraction of the emission from active galactic nuclei (AGN) arises from the accretion disk in the optical/UV bands and from the hot relativistic particles constituting the “corona.” The disk emission is of a thermal nature and can be approximated as a multi-color blackbody emission in the optical/UV band (Koratkar & Blaes 1999), while the coronal emission can extend to hard X-rays in the form of a non-thermal power-law component with a high energy cut-off (Haardt & Maraschi 1993; Fabian et al. 2015).

The emission from AGN vary strongly on a broad range of timescales and over the entire electromagnetic spectrum (see e.g., Markowitz et al. 2003; Uttley & Mchardy 2004; Breedt et al. 2010); however, the mechanism that drives this variability, and in particular the inter-band correlation, is still a subject of active research.

There has been remarkable progress in proffering explanations for this exotic variability behavior. For example, Krolik et al. (1991) argued that changes in the X-ray continuum properties, which illuminate and heat up the disk, causes the optical/UV continuum to vary. This naturally implies that the optical/UV emission should lag the illuminating X-rays in their variability (Cackett et al. 2007). This has been observed in several sources (see e.g., Cackett et al. 2007; Arévalo et al. 2009; Cameron et al. 2012; Troyer et al. 2016; Pal et al. 2017; McHardy et al. 2018). However, as pointed out by Gaskell (2007), reprocessing alone can be ruled out as the dominant mechanism of variability in many AGN through a simple energetics argument. This is because the “big blue bump” dominating the bolometric luminosity significantly exceeds the X-ray luminosity responsible for reprocessing. A few sources have shown a correlation consistent with zero or no lag, some do not reveal any correlation, and others show a more complex variability pattern (Maoz et al. 2002; Arévalo et al. 2008; Breedt et al. 2009; Pawar et al. 2017; Buisson et al. 2018). In the specific cases of NGC 5548 as well as NGC 4151, the X-ray to UV/optical relationship is complex and difficult to

explain as solely due to reprocessing (Edelson et al. 2015, 2017; Gardner & Done 2017). With respect to the inward propagation model—an alternative model—the optical/UV emission may lead the X-rays because the optical/UV photons emanate further out from the central engine. While propagation delays on viscous timescales are yet to be confirmed, the possible combination of X-ray reprocessing and propagation fluctuations on different timescales can explain the observed X-ray/optical correlations in some AGN (see e.g., Arévalo et al. 2005; Shemmer et al. 2003; Gliozzi et al. 2013).

Although it has not yet been conclusively established, Compton upscattering of optical/UV seed photons into X-rays in the hot corona can provide a compelling explanation for the optical/UV/X-ray correlated variability seen in AGN. In such a case, the thermal optical/UV seed photons drive changes in the X-ray emission. This will imply that the optical/UV seed photons lead the X-rays in their variability by the sum of light-crossing and the Comptonization timescales.

The most suitable AGN to probe the Comptonization delay are those with low black hole masses, e.g., the least-massive narrow-line Seyfert 1 (NLS1) galaxies. Mrk 493 is one such NLS1 known for its uniquely strong Fe II emission (Osterbrock & Pogge 1985). From their reverberation mapping campaign, Wang et al. (2014) measured the mass of Mrk 493 to be  $\sim 1.5 \times 10^6 M_\odot$ . We study temporal characteristics of Mrk 493 using the long *XMM-Newton* observation of Mrk 493 performed in 2015 (Bonson et al. 2018). This Letter is structured as follows. In Section 2, we describe the observation and data reduction procedure. Section 3 focuses on the data analysis and result. In Section 4, we discuss the implication of our result and conclude.

## 2. Observations and Data Reduction

The *XMM-Newton* satellite (Jansen et al. 2001) observed Mrk 493 twice in 2015, first on February 24 (observation ID 0744290201) and the second on March 2 (observation ID 0744290101), each for a duration of  $\sim 100$  ks. The observations were carried out with all European Photon Imaging Camera

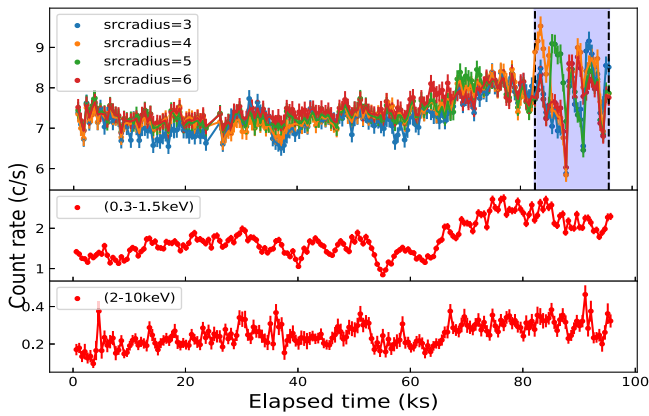


**Figure 1.** UVW1, SX, and HX light curves of Mrk 493. The UVW1 light curves were extracted with four different source radii as indicated in the panel, and the shaded blue region in the uppermost panel marks the interval containing the UVW1 frames where the source offset correction appears to be unreliable, as explained in Section 2.

(EPIC; Strüder et al. 2001; Turner et al. 2001), the Reflection Grating Spectrometer (RGS), and the Optical Monitor (OM; Mason et al. 2001). Data from the second observation (0744290101) was not used in this study because OM was operated only in the *image* mode, also several filters were used that considerably reduced the staring time for each of the used filters.

We employed the Science Analysis System (SAS v.16.1.0) package for data reduction with updated Current Calibration Files (CCFs). We generated event files for the pn and metal-oxide-semiconductor (MOS) detectors. We extracted the event file list using the task EVSELECT. The data sets were then screened individually for intervals of high particle background (i.e., flaring) in the light curve to produce good time interval (GTI) files, which were then used to obtain cleaned event lists in line with standard procedure. We did not find evidence for significant pile-up in the data. We extracted source photons from a circular region of radius  $40''$  centered on the source and the background photons from a source-free region of radius  $80''$ . We generated the background-subtracted light curve using the task EPICLCCORR. We extracted the light curve of the source in the soft X-ray (SX: 0.3–1.5 keV) and the hard X-ray (HX: 2–10 keV) bands with 500 s time bin (shown in Figure 1). We used the EPIC-pn light curves for our analysis because of its better sensitivity compared to the MOS. We used the MOS light curves only for cross-verification.

The OM observations were carried out in the *image+fast* mode using the UVW1 filter ( $\lambda_{\text{eff}} = 2910 \text{ \AA}$ ), and 25 short exposures were taken during the observation. The meta-task OMFCHAIN was used to extract the events and to generate the UVW1 light curve, again with 500 s bin size. The light curve generated is shown in the uppermost panel of Figure 1. The UVW1 light curve shows a small scale variability in the first  $\sim 80$  ks of observation, beyond which (particularly the shaded part of the light curve) it shows extreme variability with rapid decline and increase in the count rate; this is generally not expected from the accretion disk. To probe whether or not these variations are due to the source itself or to some observational artifact, we manually checked all 25 of the OM accompanying images. We noted that for a couple of frames the source was offset from the center of the detector. The maximum offset is about 25%. Although the task *ombuild*, which is a part of the

meta-task OMFCHAIN, accounts for possible missing photons for offset sources using the knowledge of the point-spread function (PSF), we decided to cross-verify this especially for the few OM frames that reveal erratic fluctuations (the shaded regions of the OM light curve in Figure 1). To do this, we imposed decreasing values of the source radius (in pixel units from 6 to 3) and generated OM light curves in each case using the command OMFCHAIN. Because less and less of the source region is expected to be offset as the source radius decreases, the generated light curves should overlap (nearly) in principle for all frames.

A close look at the uppermost panel of Figure 1 shows that the variations overlap for most of the frames as expected, except for seven frames where the fluxes show huge variations from one another (the shaded region), although with mostly similar pattern. Thus, to avoid any ambiguities we removed these frames from further analysis. This leaves us with 153 OM usable light curve data points.

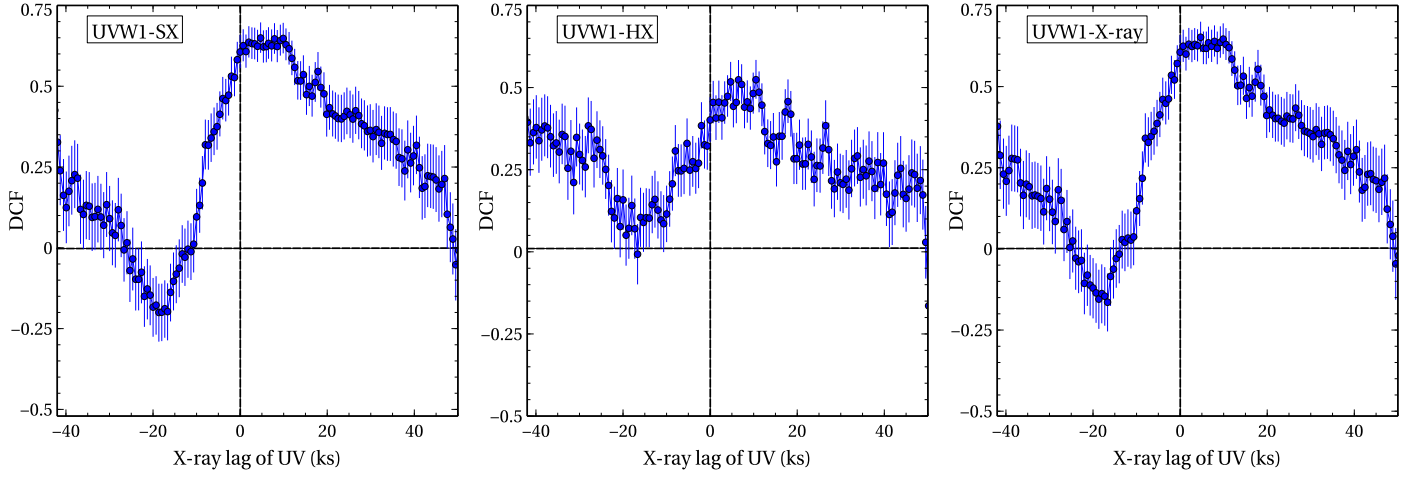
### 3. Temporal Analysis and Results

Figure 1 shows the UV, SX, and HX light curves of Mrk 493. As evident from the light curves, this AGN is very bright and highly variable. The mean count rate in the UV, SX, and HX bands are  $7.48 \pm 0.20 \text{ cs}^{-1}$ ,  $1.74 \pm 0.08 \text{ cs}^{-1}$ , and  $0.25 \pm 0.03 \text{ cs}^{-1}$ , respectively. The minimum to maximum flux ratios for the UV (excluding the shaded region in the light curve) is 1.2, while for the soft X-ray and the hard X-ray emission, the values are 3.3 and 5.5, respectively. To quantify the variability of this source, we calculated the fractional variability amplitude  $F_{\text{var}}$  (Vaughan et al. 2003), a measure of intrinsic variability in a band.  $F_{\text{var}}$  for the UV, SX, and HX bands are  $3.1 \pm 0.2\%$ ,  $23.7 \pm 0.3\%$ , and  $19.6 \pm 1.1\%$ , respectively.

We computed the cross-correlation function (CCF) between the UV and the X-ray light curves in order to probe any connection between them. We used the  $z$ -transformed discrete correlation function (ZDCF) outlined in Alexander (1997, 2013). The ZDCF method uses a variable bin size, keeping at least 11 data points per bin. We imposed 33 data points per bin in our analysis for improved statistics, and we further generated 10,000 realizations through the Markov Chain Monte Carlo (MCMC) method to estimate the lags. We carried out the analysis such that a positive time lag indicates that the variations in the UVW1 band leads. Figure 2 shows the resultant ZDCF observed between the UV and various X-ray bands. The ZDCF reveals a strong and broad peak indicating UVW1 variations are leading the X-ray bands. By applying the  $p$ -like algorithm (Alexander 2013) to the output of the ZDCF, we obtained peak likelihood lags for the UV-SX, UV-HX, and UV-full X-ray bands. These lags are given in Table 1.

To verify the detected positive lag between the UV and X-ray emission, we applied another independent popular technique for estimating lags. We computed cross-correlation function using the discrete correlation function (DCF) of Edelson & Krolik (1988) with *python* implementation (*pydcf*<sup>5</sup>). The DCFs are calculated by using a lag size of 2 ks. We constrained the DCF estimation to the lag range of  $\pm 40$  ks, as the total duration of the observation is  $\sim 100$  ks. As shown in the upper panels of Figure 3, a moderately strong correlation is detected between the UVW1 and the X-ray bands with the UVW1 emission leading by  $\sim 5$  ks, consistent with ZDCF. In estimating the time

<sup>5</sup> <https://github.com/astronomerdamo/pydcf>



**Figure 2.** ZDCF between the UVW1 and different X-rays bands: SX, HX, and the full (0.3–10 keV) band, respectively.

**Table 1**

X-Ray Lags Obtained from Cross-correlation Analysis by Different Methods

	ZDCF (ks)	DCF (ks)	JAVELIN (ks)
UV/SX	$4.7^{+4.8}_{-2.8}$	$5.5 \pm 0.05$	$4.7 \pm 0.3$
UV/HX	$10.5^{+1.0}_{-5.6}$	$7.0^a$	$7.5 \pm 0.9$
UV/X-ray	$4.7^{+4.9}_{-2.7}$	$5.5 \pm 0.04$	$4.7 \pm 0.2$

**Note.**

<sup>a</sup> We chose the mode value of the distribution due to its shape.

lag between two light curves, we calculated the mean of all DCF points that are at least 80% of the maximum. We refer to this value as  $DCF_{\max}$  and the corresponding centroid lag mean value as  $\tau_{\text{cen}}$ . This technique gave  $\tau_{\text{cen,UV/SX}} = 5.5$  ks with  $DCF_{\max,UV/SX} = 0.83$ ,  $\tau_{\text{cen,UV/HX}} = 5.2$  ks with  $DCF_{\max,UV/HX} = 0.69$  and  $\tau_{\text{cen,UV/X-ray}} = 5.5$  ks with  $DCF_{\max,UV/X-ray} = 0.81$  for the UV-SX, UV-HX, and the UV-full X-ray bands, respectively.

To estimate the significance of the detected lag, we implemented the Monte Carlo method described in Peterson et al. (1998). We created 10,000 pairs of synthetic light curves using the random subset selection (RSS) technique outlined in Peterson et al. (1998) and then calculated the DCF of each pair. The dashed blue lines in the upper panels of Figure 3 show the 90% confidence limit on the estimated lags. Following the same approach as with the observed light curves, we computed the centroid lag value for each pair of simulated light curves  $\tau_{\text{cen,sim}}$  and the corresponding  $DCF_{\max,sim}$ . With these values, we constructed the sample distribution function of  $\tau_{\text{cen,sim}}$  i.e., the cross-correlation peak distribution (CCPD) of lags. The resulting distributions are shown in the lower panels of Figure 3 and the measured values (from Gaussian fit) are quoted in Table 1. The fact that they show good agreement with ZDCF supports our claim that the X-ray emission lag the UVW1 emission by  $\sim 5$  ks.

To further validate our lag estimation, we employed the JAVELIN<sup>6</sup> code of Zu et al. (2011). Lags estimated from this method are shown in Figure 4. By assuming a perfect Gaussian distribution of lags (depicted by the red dashed lines in the plots), we computed the mean and  $1\sigma$  error on the lags to be  $4.7 \pm 0.3$  ks,  $7.5 \pm 0.9$  ks, and  $4.7 \pm 0.2$  ks, respectively, for

the UV-SX, UV-HX, and the UV-X-ray (also shown in Table 1).

## 4. Discussion and Conclusion

We analyzed the  $\sim 100$  ks simultaneous *XMM-Newton* UV and X-ray data of the narrow-line Seyfert 1 galaxy Mrk 493 to search for possible correlated variability between these two bands. We found a significant correlation between these bands in which the UV emission lead the X-rays in their variability by  $\sim 5$  ks. We investigate the origin of the observed lags below.

### 4.1. Accretion Disk Timescales

If the dominant emission from the accretion disk is a result of viscous heating in the disk, the photons emanating from different radii can be described as blackbodies with different temperatures (Netzer 2013).  $\lambda_{\text{eff}}$  can be converted to the blackbody temperature, which peaks in the particular band. Comparing this temperature to that of a standard accretion disk, we can calculate the disk radius and, subsequently, the light-crossing time between the X-ray source and the region of the disk waveband with peak wavelength ( $\lambda_{\text{eff}}$ ) as

$$t_{\text{lc}} \approx 2.6 \times 10^5 \left( \frac{\lambda_{\text{eff}}}{3000 \text{ \AA}} \right)^{4/3} \left( \frac{\dot{M}}{\dot{M}_{\text{Edd}}} \right)^{1/3} \left( \frac{M_{\text{BH}}}{10^8 M_{\odot}} \right)^{2/3}. \quad (1)$$

The dynamical timescale corresponding to the Keplerian frequency can be written as

$$t_{\text{dyn}} = \left( \frac{r^3}{GM_{\text{BH}}} \right)^{1/2} \approx 500 \left( \frac{M_{\text{BH}}}{10^8 M_{\odot}} \right) \left( \frac{r}{r_g} \right)^{3/2}. \quad (2)$$

The thermal timescale  $t_{\text{th}}$  can be written, assuming thermal equilibrium in the disk, as

$$t_{\text{th}} = \frac{1}{\alpha} t_{\text{dyn}}, \quad (3)$$

and finally, because the radial inflow of matter is governed by viscosity, the viscous timescale  $t_{\text{vis}}$  can be expressed as

$$t_{\text{vis}} \approx \frac{1}{\alpha} \left( \frac{r}{h} \right)^2 t_{\text{dyn}}, \quad (4)$$

<sup>6</sup> <https://bitbucket.org/nye17/javelin>

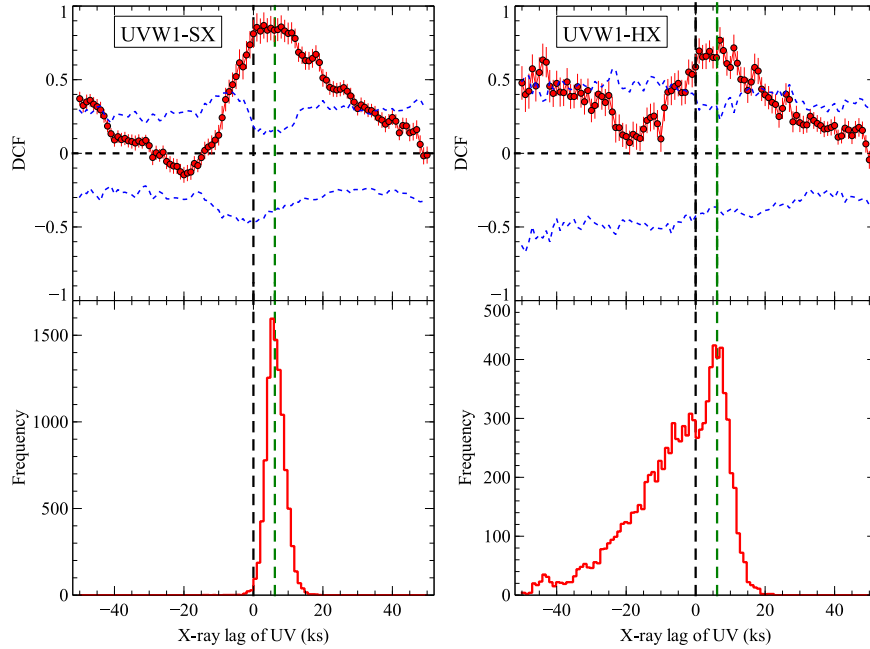


**Figure 3.** Upper panels: the DCF between the UVW1-SX and the UVW1-HX bands obtained using the method described in Edelson & Krolik (1988). Lower panels: time lag distribution based on 10,000 simulated light curves using the *bootstrap* technique.

where  $r$  and  $h$  are the radius and height of the disk, respectively.  $\alpha \sim 0.1$  is the viscosity parameter, and  $r_g = GM_{\text{BH}}/c^2$ .

For Mrk 493 with  $M_{\text{BH}} \sim 1.5 \times 10^6 M_{\odot}$  (Wang et al. 2014), assuming a moderately high Eddington scaled accretion rate of 0.1, we calculated the various timescales associated with the accretion disk. We used  $\lambda_{\text{eff}}$  of the UVW1 filter as 2910 Å (Mason et al. 2001). Our estimated values for the different timescales are  $t_{\text{lc}} \sim 7.0$  ks,  $t_{\text{dyn}} \sim 2.5$  days,  $t_{\text{th}} \sim 25$  days, and  $t_{\text{vis}} \sim 7$  years.

#### 4.2. Propagation Fluctuation Delay

The broadband variability properties of many accreting systems are usually explained in terms of inward propagating fluctuations in the accretion disk (see e.g., Lyubarskii 1997; Arévalo & Uttley 2006). In this model, the hot inner regions emitting soft X-rays and the outer cooler part of the disk responsible for the longer-wavelength UV photons cannot exchange information faster than the sound crossing time  $t_{\text{sc}}$ . For accretion rate fluctuations propagating inward in the radial direction, the sound crossing time can be written as

$$t_{\text{sc}} = t_{\text{dyn}} \left( \frac{r}{h} \right), \quad (5)$$

where  $h$  is disk height and  $r$  is the radius corresponding to the observed UV emission. We assumed  $h/r \sim 0.1$  (see e.g., Czerny 2006) for this source, thus the fluctuation propagation timescale is of the order of  $\sim 2.2 \times 10^6$  s. This is about two orders of magnitude longer than our measured UV/X-ray lag. Therefore, we rule out accretion rate fluctuation propagating inward through the disk as being the possible origin of our measured UV/X-ray lag.

#### 4.3. Comptonization Lag

Although the light-crossing timescale provides a reasonable explanation for the detected lag, the Comptonization process itself requires a finite time due to multiple Compton upscattering. Consequently, the observed delay should be the combination of the light-crossing time  $t_{\text{lc}}$  plus the time it will take for the soft photons to be Comptonized in the hot electron plasma, i.e., the Comptonization time  $t_{\text{comp}}$  (see, e.g., Zdziarski 1985; Dasgupta & Rao 2006; Dewangan et al. 2015). A seed photon injected into a static Comptonizing corona with a small optical depth  $\tau$  ( $\tau \ll 1$ ) and electron temperature  $kT_e$  increases its energy by a fraction

$$A = 1 + 4\theta + 16\theta^2, \quad (6)$$

where  $\theta = \frac{kT_e}{m_e c^2}$ ,  $k$  is the Boltzmann's constant, and  $m_e$  is the mass of an electron. If the injected photon undergoes  $n$  scatterings within the cloud before it escapes, its final energy is  $E_n = A^n E_0$ , where  $E_0$  is the initial energy of the injected photon.

If the size of the X-ray emitting corona is  $R_c$ , then the photon mean free path  $\lambda$  through the cloud can be expressed as  $\lambda \sim \frac{R_c}{\max(1, \tau)}$ . Thus, the time interval between successive scatterings can be expressed as  $t_c = \frac{(R_c/c)}{\max(1, \tau)}$ .

Finally, the Comptonization time  $t_{\text{comp}}$  required to upscatter a seed photon with energy  $E_0$  to  $E_n$  after  $n$  scatterings will be

$$t_{\text{comp}} = nt_c. \quad (7)$$

For Mrk 493, we considered a plausible scenario where UVW1 seed photons produced due to viscous heating in the disk are Compton upscattered into the observed X-rays after traveling the light-crossing time  $t_{\text{lc}}$  to reach the compact corona of size  $\sim 20r_g$  (see e.g., Reis & Miller 2013; Adegoke et al. 2017). We took the UV seed photon energy to be  $\sim 4.25$  eV (for  $\lambda_{\text{eff}} = 2910$  Å). Therefore, the time it will take to increase

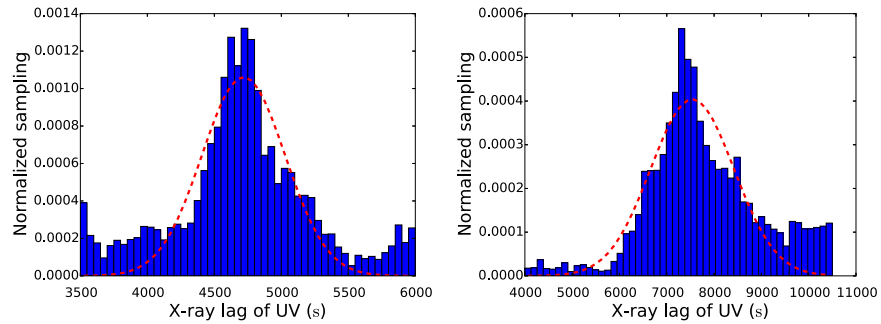


**Figure 4.** From left to right: JAVELIN cross-correlation plot between SX and the UVW1 energy bands and HX and UVW1 bands.

the energy of this photon to  $\sim 1.0$  keV (the approximate soft X-ray midpoint energy) due to inverse Compton scattering in an electron cloud corona with  $T_e \sim 100$  keV, as calculated from the above relation, will be  $\sim 900$  s, while it will take  $\sim 1200$  s to increase the seed photon's energy to 5 keV (i.e., the approximate midpoint energy of the hard X-rays). This difference in Comptonization delay is expected, as more scatterings will be required for the injected seed photon to be boosted to harder X-ray energies. Then, as stated above, the UV/X-ray time lag  $t_{\text{lag}}$  should be

$$t_{\text{lag}} = t_{\text{lc}} + t_{\text{comp}} \quad (8)$$

For  $\dot{m} = 0.1$ , the expected lag from the above equations should be  $\sim 7.9$  ks and  $\sim 8.2$  ks for the UV-SX and UV-HX flux variabilities, respectively. These values are in good agreement with our measured values within measurement uncertainties as shown in Table 1. Even for a super-Eddington accretion rate with  $\dot{m} \sim 1.0$ , the predicted value of lag will be  $\sim 16$  ks, only about a factor of 3 higher than our estimated lag.

Recent work on the *XMM-Newton* X-ray data of Mrk 493 by Bonson et al. (2018) suggests the presence of strong reflection components and posits that the variations in X-rays are due to the changes in the degree of light bending in the vicinity of the central black hole. Therefore, one might expect the production of UV emission from thermal reprocessing of the illuminating X-rays in which the UV lag the X-rays. The absence of such a lag in our analysis implies that reprocessing probably does not play an important role in the UV/X-ray variability seen in this source. The most likely scenario is that, due to strong light-bending effect, strong coronal illumination is confined to the inner regions with no reprocessed emission in the UV band. This will be the case if the coronal height is considerably small (also suggested by Bonson et al. 2018). Thus, the observed delay can most plausibly be explained as Comptonization lag.

We note that  $\sim 3\%$  variability amplitude in the optical/UV band is unlikely to drive  $\sim 20\%$  variability amplitude in the X-rays by thermal Comptonization alone in a static corona. The 0.3–10 keV band emission consists of the primary power law arising from the thermal Comptonization, the soft X-ray excess, and the reflection. The latter two components can introduce additional variability. If we filter out the rapid variability events in the 2–5 keV band light curve, which is relatively free of soft excess and iron line, the variability amplitude becomes comparable to that of the UVW1 band. This shows that variations in the seed UV photons primarily drives the slower variability of the X-ray power-law continuum. The soft X-ray excess can arise either due to thermal Comptonization in a warm, optically thick material (most likely the innermost

regions of the disk itself), and/or blurred reflection. In the warm Comptonization scenario, if the soft excess and the UV emission arise from the adjacent regions (see e.g., Kubota & Done 2018), the soft X-ray excess can increase both due to increased seed photons and increased energy dissipation in the warm corona. Therefore, the soft band can probably vary strongly and still be correlated with the UV.

We thank Banibrata Mukhopadhyay, Iossif Papadakis, and the anonymous referee for useful input that improved the manuscript. O.A. and M.P. acknowledge support from IUCAA and the DSKPDF program of UGC, India, respectively.

#### ORCID iDs

Oluwashina Adegoke <https://orcid.org/0000-0002-5966-4210>  
 Gulab C. Dewangan <https://orcid.org/0000-0003-1589-2075>  
 Pramod Pawar <https://orcid.org/0000-0003-3188-1501>

#### References

- Adegoke, O., Rakshit, S., & Mukhopadhyay, B. 2017, *MNRAS*, **466**, 3951  
 Alexander, T. 1997, *ASSL*, **218**, 163  
 Alexander, T. 2013, arXiv:1302.1508  
 Arévalo, P., Papadakis, I., Kuhlbrodt, B., & Brinkmann, W. 2005, *A&A*, **430**, 435  
 Arévalo, P., & Uttley, P. 2006, *MNRAS*, **367**, 801  
 Arévalo, P., Uttley, P., Kaspi, S., et al. 2008, *MNRAS*, **389**, 1479  
 Arévalo, P., Uttley, P., Lira, P., et al. 2009, *MNRAS*, **397**, 2004  
 Bonson, K., Gallo, L. C., Wilkins, D. R., & Fabian, A. C. 2018, *MNRAS*, **477**, 3247  
 Breedt, E., Arévalo, P., McHardy, I. M., et al. 2009, *MNRAS*, **394**, 427  
 Breedt, E., McHardy, I. M., Arévalo, P., et al. 2010, *MNRAS*, **403**, 605  
 Buisson, D. J. K., Lohfink, A. M., Alston, W. N., et al. 2018, *MNRAS*, **475**, 2306  
 Cackett, E. M., Horne, K., & Winkler, H. 2007, *MNRAS*, **380**, 669  
 Cameron, D. T., McHardy, I., Dwelly, T., et al. 2012, *MNRAS*, **422**, 902  
 Czerny, B. 2006, in ASP Conf. Ser. 360, AGN Variability from X-Rays to Radio Waves, ed. C. M. Gaskell et al. (San Francisco, CA: ASP), 265  
 Dasgupta, S., & Rao, A. R. 2006, *ApJL*, **651**, L13  
 Dewangan, G. C., Pawar, P. K., & Pal, M. 2015, in ASI Conf. Ser. 12, Recent Trends in the Study of Compact Objects (RETCO-II): Theory and Observation, ed. I. Chattopadhyay et al. (Pune: BASI), 57  
 Edelson, R. A., & Krolik, J. H. 1988, *ApJ*, **333**, 646  
 Edelson, R., Gelbord, J., Cackett, E., et al. 2017, *ApJ*, **840**, 41  
 Edelson, R., Gelbord, J. M., Horne, K., et al. 2015, *ApJ*, **806**, 129  
 Fabian, A. C., Lohfink, A., Kara, E., et al. 2015, *MNRAS*, **451**, 4375  
 Gardner, E., & Done, C. 2017, *MNRAS*, **470**, 3591  
 Gaskell, C. M. 2007, in ASP Conf. Ser. 373, The Central Engine of Active Galactic Nuclei, ed. L. C. Ho & J.-W. Wang (San Francisco, CA: ASP), 596  
 Gliozzi, M., Papadakis, I. E., Grupe, D., Brinkmann, W. P., & R ath, C. 2013, *MNRAS*, **433**, 1709  
 Haardt, F., & Maraschi, L. 1993, *ApJ*, **413**, 507  
 Jansen, F., Lumb, D., Altieri, B., et al. 2001, *A&A*, **365**, L1  
 Koratkar, A., & Blaes, O. 1999, *PASP*, **111**, 1  
 Krolik, J. H., Horne, K., Kallman, T. R., et al. 1991, *ApJ*, **371**, 541

- Kubota, A., & Done, C. 2018, *MNRAS*, 480, 1247
- Lyubarskii, Y. E. 1997, *MNRAS*, 292, 679
- Maoz, D., Markowitz, A., Edelson, R., & Nandra, K. 2002, *AJ*, 124, 1988
- Markowitz, A., Edelson, R., Vaughan, S., et al. 2003, *ApJ*, 593, 96
- Mason, K. O., Breeveld, A., Much, R., et al. 2001, *A&A*, 365, L36
- McHardy, I. M., Connolly, S. D., Horne, K., et al. 2018, *MNRAS*, 480, 2881
- Netzer, H. 2013, *The Physics and Evolution of Active Galactic Nuclei* (Cambridge: Cambridge Univ. Press)
- Osterbrock, D. E., & Pogge, R. W. 1985, *ApJ*, 297, 166
- Pal, M., Dewangan, G. C., Connolly, S. D., & Misra, R. 2017, *MNRAS*, 466, 1777
- Pawar, P. K., Dewangan, G. C., Papadakis, I. E., et al. 2017, *MNRAS*, 472, 2823
- Peterson, B. M., Wanders, I., Horne, K., et al. 1998, *PASP*, 110, 660
- Reis, R. C., & Miller, J. M. 2013, *ApJL*, 769, L7
- Shemmer, O., Uttley, P., Netzer, H., & McHardy, I. M. 2003, *MNRAS*, 343, 1341
- Strüder, L., Briel, U., Dennerl, K., et al. 2001, *A&A*, 365, L18
- Troyer, J., Starkey, D., Cackett, E. M., et al. 2016, *MNRAS*, 456, 4040
- Turner, M. J. L., Abbey, A., Arnaud, M., et al. 2001, *A&A*, 365, L27
- Uttley, P., & McHardy, I. M. 2004, *PThPS*, 155, 170
- Vaughan, S., Edelson, R., Warwick, R. S., & Uttley, P. 2003, *MNRAS*, 345, 1271
- Wang, J.-M., Du, P., Hu, C., et al. 2014, *ApJ*, 793, 108
- Zdziarski, A. A. 1985, *ApJ*, 289, 514
- Zu, Y., Kochanek, C. S., & Peterson, B. M. 2011, *ApJ*, 735, 80